ELSEVIER

Contents lists available at ScienceDirect

Advances in Water Resources

journal homepage: www.elsevier.com/locate/advwatres





Identifying the source settings of deep brine leakage from CO₂ geological repositories using observations from shallow overlying formations

Ahmad H. Askar^{a,*}, Jeremy T. White^b, Tissa H. Illangasekare^c

- a INTERA Inc. Boulder, CO, USA
- ^b INTERA Inc. Perth, Australia
- c Center for Experimental Study of Subsurface Environmental Processes, Department of Civil and Environmental Engineering, Colorado School of Mines, CO, USA

ARTICLE INFO

Keywords: Carbon storage Ensemble-based data-assimilation Contaminant source identification Brine leakage

ABSTRACT

Shallow groundwater resources overlaying deep saline formations used in carbon storage applications are subjected to a potential contamination threat by CO₂/brine leakage via natural or anthropogenically-induced conductive pathways in the confining caprock. Identifying the leakage source location and rate is critical for developing remediation plans and designing corrective actions. Owing to limited information about the flow and transport characteristics of deep regimes and high cost of obtaining data on their response to CO2 injection operation, estimating accurate source settings (i.e., location and rate) can be extremely challenging. Under such conditions, Bayesian inverse frameworks become useful tools to help identify potential leakage patterns. This study tests and validates an ensemble-based data-assimilation approach that reduces the uncertainty in the prior knowledge about source settings through conditioning forward transport models using relatively inexpensive easy-to-acquire shallow zone data. The approach incorporates the newly developed ensemble smoother tool in the inversion code "PEST++" with the transport code "FEFLOW" to perform history matching and uncertainty analysis. A novel parameterization method that allows the disposition of potential source was used to search the leakage location during calibration process. In the absence of field data, the approach was validated using experimental data generated in ~8 m long soil tank simulating leakage from storage zone migrating to the shallow aquifer. The results show that source location uncertainty can be reasonably reduced using shallow zone data collected from near-surface aquifers. However, more prior information about the system and deeper data are essential to estimate a practical probability range for the leakage rate.

1. Introduction

 ${\rm CO}_2$ concentrations in the atmosphere have crossed a new climate-change threshold in 2023 by reaching +419 ppm (SIO, 2023), which adversely contributes to the global warming of the earth (Ajayi et al., 2019; Celia et al., 2015). It has been estimated that 440 ± 20 gigatons of carbon (1015 gs) were emitted as ${\rm CO}_2$ to the atmosphere from 1850 to 2018 due to fossil fuel burning (Friedlingstein et al., 2019). Carbon geologic sequestration (CGS) has been recognized as one of the promising strategies that can reduce ${\rm CO}_2$ loadings to the air while maintaining the use of fossil fuels as a main source of energy (IPCC, 2005; Lackner, 2003; Bachu, 2003; U.S. DOE, 2015; Looney, 2020). CGS technology involves capturing the ${\rm CO}_2$ at the source (e.g., power plants) and then injecting it into deep geological formations under high pressure. Deep saline formations represent ideal ${\rm CO}_2$ repositories among all

geological options because of their abundance and enormous storage capacity (Grobe et al., 2009). CO_2 injection pressure poses a leakage risk from natural or induced conductive pathways (i.e., faults or fractures) in the confining caprock, which threatens the water quality in the shallow aquifers that are used as potable resources (Gasda et al., 2004; Rutqvist et al., 2007; 2008; Celia et al., 2011).

Identifying the leakage source location and rate is essential for effective planning, designing and implementation of corrective actions and remediation measures (Jung et al., 2013). Various approaches have been discussed in the literature to characterize the contaminant source settings through optimization, analytical, direct, probabilistic, and inverse methods (Atmadja and Bagtzoglou, 2001). Of particular interest to this study are the approaches that identify the contaminant source location and reproduce its release history, which can be found in Gorelick et al. (1983), Wagner (1992), Skaggs and Kabala (1995), Dimov

E-mail address: ahmedaskar6@gmail.com (A.H. Askar).

^{*} Corresponding author.

et al. (1996), Neupauer and Wilson (1999; 2001; 2002), Mahar and Datta (2000), Atmadja and Bagtzoglou (2001), Mahar and Datta (2001), Aral et al. (2001), Singh et al. (2004), Mahinthakumar and Sayeed (2005), Neupauer and Lin (2006), Singh and Datta (2007), and Srivastava and Singh (2014). The challenge with implementing any of these methods to characterize the deep leakage source settings in CGS projects is the scarcity and low accuracy of available prior information about the geological and transport properties of the system. These conditions make most of the modeling parameters and boundary conditions (BCs) uncertain, which exponentially enlarge the inverse problem dimensions, hindering the applicability of certain Bayesian inverse frameworks due to scalability issues (Knowling et al., 2019; Wu et al., 2020; Omagbon et al., 2021; Kugler et al., 2022). In the same context, Milnes and Perrochet (2007) emphasized the necessity of acquiring detailed information about the velocity and transport parameters of the system as well as accurate BCs to reasonably estimate the contaminate source settings using such classical optimization approaches, which can be practically infeasible in the case of CGS sites.

For CGS applications, different monitoring techniques have been developed and applied to detect any anomaly in the pressure and water quality in the shallow and deep overlying formations that indicate CO₂/ brine leakage event (Ajayi et al., 2019; Vermeul et al., 2016; NETL, 2017). Due to cost and safety constraints, while a comparatively large number of monitoring wells are usually available in the shallow aquifer, a limited number of sensors can be placed in the deep overlying formations (Nordbotten et al., 2004; Tsang et al., 2008; Hovorka et al., 2013; Vermeul et al., 2016). Therefore, an approach that can appropriately and rigorously utilize the available shallow data in CGS sites to reduce the uncertainty in the system properties and identify the leakage source location and rate is needed for developing remediation and mitigation plans in case a leakage event occurs. This approach should also be able to deal with both uncertainties in field-data and prior information about the hydraulic and structural configuration of the deep formations (e.g., heterogeneity of the storage zone permeability and caprock-fracture structure).

Lately, researchers have started to use the technique of ensemble smoothing in the history matching of contamination data and source identification due to its scalability and efficiency in handling high dimensional parameter spaces of real-world class models (Todaro et al., 2021; LIU et al., 2021; Jiang et al., 2022; Xu et al., 2022; Zheng et al., 2022; Chen et al., 2022). White (2018) incorporated the method of ensemble smoothing in PEST++ (i.e., PESTPP-IES) to enable the quantification of uncertainty in calibrated model parameters and predicted system behaviors while maintaining a reasonable computational effort (White et al., 2020). PESTPP-IES tool was recently applied to address different groundwater problems associated with a considerable margin of uncertainty in available information, such as evaluating the risk of groundwater contamination by conventional gas development (Rassam et al., 2022), delineating the probabilistic recharge areas of priority water-supply wells (Fienen et al., 2022), and quantifying the uncertainty in the predicted production-pressures and temperatures high-enthalpy geothermal reservoirs (Bjarkason et al., 2020).

A few synthetic-data-based studies that utilized different data assimilation techniques to identify and evaluate CO₂/brine leakage risk were found in literature. González-Nicolás et al. (2015) used the single iteration ensemble smoother (SIES) and restart ensemble Kalman filter techniques with pressure data, collected from the caprock top surface, to locate permeable conductive pathways. The authors attributed the poor performance of the SIES to the fact that the code adjusts the parameter ensemble in a single comprehensive data assimilation step, which does not allow the parameter ensemble to evolve gradually over multiple iterations. Moreover, the authors pointed out the challenges of assimilating data to a non-gaussian permeability field that represent caprock discontinuities. Cameron et al. (2016) incorporated a particle swarm optimization tool with above-zone pressure data to estimate the size and location of CO₂ leaky pathways. Sun and Durlofsky (2019) applied a

data-space inversion method to predict the CO_2 plume location within the storage unit using pressure and CO_2 saturation data. Ma et al. (2019) also used pressure and CO_2 saturation data but with time-lapse seismic data in an ensemble Kalman filter inversion framework to estimate the storage formation hydraulic properties and predict CO_2 migration. Tadjer A. and Bratvold R. B. (2021) combined a Bayesian evidential learning protocol with data-space inversion to reduce uncertainty in the predicted CO_2 mass in the storage formation and its corresponding leakage risk using CO_2 saturation data.

This study aims to test and evaluate the efficacy of using PESTPP-IES as a tool for characterizing the source settings of brine leakage from CO2 repositories using easily-available, comparatively inexpensive shallow data only. Source identification comprises determining the most probable range of leakage location in the caprock and leakage rate that are both essential for remediation studies. In related and similar studies, where field data was not available (Keating et al. 2010) and synthetic data representation of leakage process can be questionable for such testing and validation, researchers used intermediate scale test systems to generate high-resolution experimental data (Luyun Jr et al., 2011; Trevisan et al., 2017; Agartan 2015; Askar et al., 2021a). In this study, we applied the same method of using data produced in a lab experiment, conducted in a soil tank mimicking brine leakage from a CO2 storage formation (Askar et al., 2021a). The brine migration in the tank was numerically simulated using a flow and transport model developed using the finite element transport code of FEFLOW (Diersch, 2014), which was then utilized as a forward base-model under PESTPP-IES for history matching and uncertainty analysis (UA). The testing and validation analysis included multiple scenarios for both system information uncertainty (i.e., hydraulic, and structural settings of the storage zone and fractured caprock) and spatial data resolution (i.e., shallow, and relatively deep data).

2. Methods and approaches

This section presents a brief description of the experimental system where data was generated. In addition, the forward model setup, parameterization, data assimilation, and UA methods, as well as testing-scenarios are discussed.

2.1. Experimental data

Data used in this study is a subset of a dataset generated by Askar et al. (2021a) using an ~8 m long soil tank, where brine leakage migration from a storage unit (Zone 1) to a shallow aquifer (Zone 3) across multiple intermediate layers (Zone 2) was simulated (Fig. 1). A thick plexiglass sheet, with six openings, was placed to separate Zones 1 and 2 representing the fractured caprock. Askar et al. (2021a) used a horizontal soil tank to simulate the vertical plume migration in the field, as it was not feasible to set up a vertical tank in the laboratory. In this test configuration, to minimize the density contrast between the leakage plume and the background water, thus eliminating any potential density-driven flow, a low-concentration NaBr solution was used as a brine surrogate. The NaBr tracer was introduced to the system through the lowest injection port in the tank (marked by a red circle in Fig. 1). The tank was heterogeneously packed following specific architectures of designed correlated random fields of sand permeability. More information about the experiment conceptualization, tank struction/assembly and system design can be found in Askar et al. (2021a).

In the experiment, four different boundary conditions (BCs) were assigned at the top and bottom boundaries of both ends of the tank to produce the required flow-field across the three zones; constant-head and no-flow BCs were assigned to the top and bottom ends of Zone 1, respectively. While constant-head and constant-flux BCs were prescribed for the top and bottom ends of Zone 3, respectively. A no-flow BC was used with the outlet of Zone 1 to represent a screen that was clogged

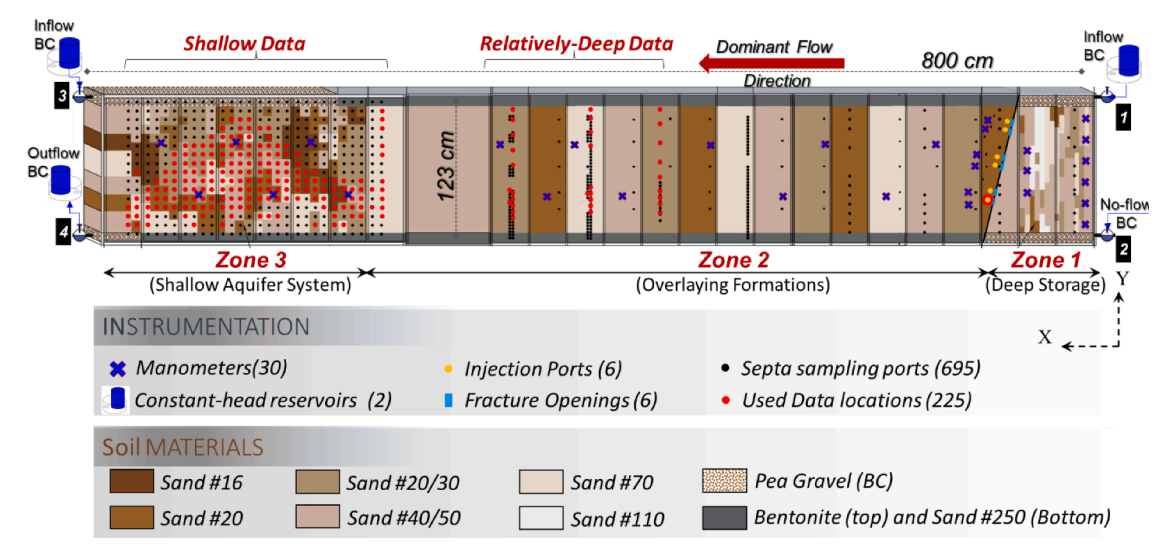


Fig. 1. Schematic demonstrating the location of experimental data (red dots) as well as the experiment setup, including the packing heterogeneity and tank instrumentation, used to generate this data (modified after Askar et al. (2021b)). Note, the flow occurs from right to left.

by fine particles and rust during the experiment (Askar et al., 2021a). Those BCs generated a flow-field that included relatively vertical flows in Zones 1 and 3 and horizontal flow across Zone 2.

The subset of experimental data used in this study comprised timeseries of hydraulic heads and plume concentrations, collected from 30 monuments and 205 sampling ports in the tank, respectively (manometers and sampling ports are respectively marked by blue-crosses and red-dots in Fig. 1). As the experiment was running under steady-state flow conditions (Askar et al., 2021a), the twice-a-day collected head readings from each manometer were almost constant, thus average values over time were used to represent the system hydraulic head at each manometer location during the experiment.

On a different note, the aqueous samples were not taken on a constant-interval basis, but rather when the dyed tracer was seen to approach a septa port location using the transparent side of the tank (Askar et al., 2021a). Such sampling strategy allowed for developing smooth breakthrough curves of NaBr at each port location. Approximately a period of 190 h was required to run the experiment and develop such dataset. It should be noted that the data was divided into two groups based on their locations; shallow data points in Zone 3 and relatively-deep data points in the shallow part of Zone 2 (Fig. 1), to investigate the sensitivity of source identification results to data location.

2.2. Base-Model setup

The model described herein is referred to as the "base-model", which can be seen as a numerical testbed for different uncertainty scenarios in the prior knowledge of the system so that we can evaluate the efficacy of source identification using the proposed method under various degrees of field data scarcity and lack of information.

A 2D base-model (with steady-state flow and transient transport conditions) was developed using FEFLOW to simulate the brine migration across the experimental tank and to underlie PESTPP-IES as a forward model during history-matching and UA. The model domain was spatially discretized using 134.5~K elements with an average area of approximately $0.37\pm0.32~cm^2$ to cover the full dimensions of the tank. In the source vicinity, the model mesh was significantly refined to reduce the grid-Péclet number and thus ensure low numerical dispersion (smallest element size was about $1.24E-04~cm^2$). Moreover, such high-resolution of spatial discretization at the source area allows for high precision in source location identification using the proposed approach.

The base-model space discretization, including mesh refinements,

was carefully implemented to maintain a reasonable run time of the transient model, hence enabling the formulation of a highly parameterized inverse problem that is necessary for the UA analysis. Moreover, the predictor-corrector time integrator algorithm, introduced by Gresho et al. (1979) and improved by Bixler (1989), was used to implement a reasonably high-resolution of time discretization, particularly in early simulation times, while maintaining a small total run time for the model (i.e., \sim 2.2 mins). Additional time steps were added to the model to acquire the simulation results at the recorded times of head and concentration data.

Similar BCs to those applied in the experiment were prescribed in the base-model using Dirichlet and Neuman BC types with values shown in Fig. 2. The sand packing configurations of the tank's three zones were explicitly represented in the base-model. The initial hydraulic and transport properties (i.e., hydraulic conductivity (K), porosity, and dispersivity) of the sand media were defined in the base-model using the calibrated values presented by Askar et al. (2021a). It is important to emphasize that such initial values have been changed according to the uncertainty scenario under study. For example, to address a scenario where limited knowledge about the permeability field of the storage formation is available, Zone 1 in the model was re-parameterized using pilot-points (pp) with initial Ks based on column-scale experiments for the sand types used in Zone 1 (i.e., non-calibrated values).

2.3. Source identification approach

The following steps were adapted to characterize the contamination source (i.e., location and rate): (1) PESTPP-IES was connected to the "base-model" via standard PEST-style model-interface files, (2) prior probability density functions (PDFs) were defined for model parameters pertained to each uncertainty scenario, (3) a set of equally-likely realizations (i.e., prior ensemble) were generated by PESTPP-IES by randomly sampling the defined PDFs, and (4) finally, PESTPP-IES iteratively modifies the ensemble of parameter realizations through history matching using the ensemble smoothing technique to produce a posterior parameter ensemble. By that, the most probable range of source location and leakage rate (i.e., narrowest range) can be statistically estimated simultaneously with other (uncertain) model parameters, so that any non-identifiabilities/non-uniqueness between the estimated source settings and other uncertain model parameters can be rigorously represented. It should be noted that the prior PDFs of all model parameters were described using a gaussian distribution with a standard deviation determined by dividing the distance between the parameters'

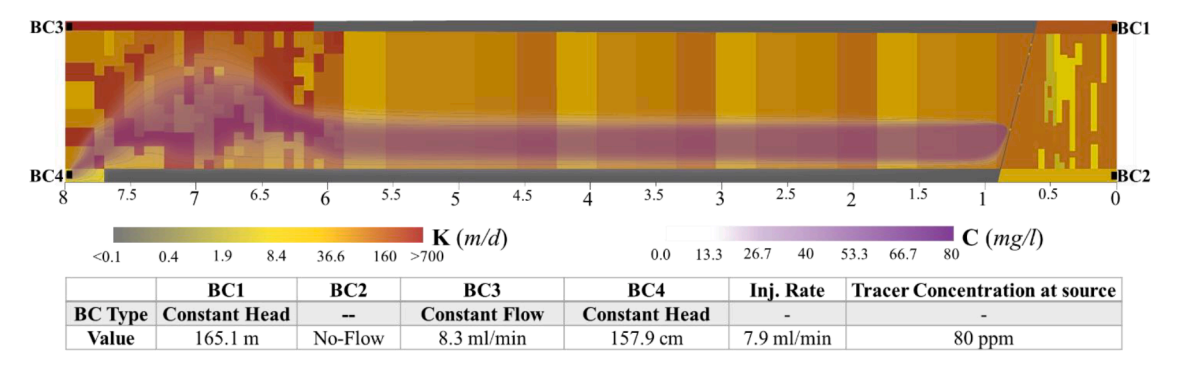


Fig. 2. Base-model setup including hydraulic properties, initial and boundary conditions.

upper and lower bounds by four (i.e., 95% confidence interval). The theory underpinning PESTPP-IES process can be found in White (2018) and White et al. (2020).

For this analysis, different modeling workflow tools were incorporated, including PESTPP-IES, pyEMU and FEFLOW-IFM to develop an automated and reproducible workflow that parameterizes the base-model according to the uncertainty scenario to be addressed, then run PESTPP-IES and finally, plot the results. pyEMU, a Python package that enables defining the inputs, running, and postprocessing all PEST++ uncertainty analyses (White et al., 2016), was used to retrieve and plot the recorded model results of interest from the PESTPP-IES output files. FEFLOW-IFM, a Python programming Interface for FEFLOW, was used to facilitate model parameterization under each uncertainty scenario, run the model under PESTPP-IES and retrieve model results.

2.4. Uncertainty scenarios and data-availability cases

Multiple uncertainty scenarios were developed to examine the capability of available observation data to appropriately characterize source settings under different parameterization scenarios, where each parameterization scenario represents a possible inverse problem design regarding what model inputs are treated as "uncertain". Testing different parameterization scenarios enabled us to reasonably identify the most critical information related to uncertain model inputs needed to characterize the source. Table 1 presents eight uncertainty scenarios developed for this analysis to test the influence of various sources of model input uncertainty on the resulting ability to resolve the source settings in a Bayesian framework. It should be noted that the 8th scenario represents the ideal case of having complete knowledge about the system, which was treated as a reference scenario for evaluating the results from the rest. For all parameterization scenarios, the injection source location and rate were treated as "uncertain" using the same prior parameter. Model inputs that were excluded from a given scenario were held constant at the calibrated values described in Askar et al. (2021a).

In addition to the parameterization scenarios, two distinct calibration datasets, containing observations from different distances from the source were used to test the sensitivity of source identification accuracy to the location of available data. The first tested dataset, referred to here as "shallow data" includes concentration measurements collected from

Table 1 Tested uncertainty scenarios.

Scenario #	o # Uncertain model inputs					
1	Storage zone flow field/gradient + Source settings					
2	Storage zone permeability field + Source settings					
3	Caprock fracture settings + Source settings					
4	Overlaying formations' permeabilities + Source settings					
5	Overlaying formations' porosities + Source settings					
6	Model dispersivity + Source settings					
7	All above model inputs + Source settings					
8	Source settings only					

Zone 3 only (representing the easily available data from the near-surface aquifers in the field, which can typically be collected in high spatial resolution). While the second tested dataset, referred to here as "relatively-deep data" includes deeper concentration measurements collected from the shallow part of Zone 2. This dataset represents the collected data using comparatively deep sensors that may exist in shallow overlying formations. Two data-availability cases were evaluated in this study, the first included the shallow dataset only, while the second included both shallow and relatively-deep datasets. It is worth mentioning that both cases included head measurements from the three zones in the tank (i.e., across the entire system depth), as the latest advances in monitoring technologies and geophysical techniques allow for reasonably mapping the pressure field inside and over the CO₂ storage formation (U.S. EPA, 2013; Zhou et al., 2016; NETL, 2017; Mortezaei et al., 2018).

2.5. Parameterization and prior definition

Various degrees of knowledge about aquifer properties were assumed for the shallow (Zone 3) and deep formations (Zone 2 and 1). Full knowledge about the hydraulic properties and heterogeneity architecture of Zone 3 was assumed known to focus the data-assimilation process and fully utilize the information content of the data towards characterizing the source settings instead of calibrating Zone 3 parameters/properties that are not among our interest in this analysis. Particularly that shallow aquifers (Zone 3) can be characterized separately (away from this analysis) with reasonable cost using numerous investigation techniques that cannot be applied to deep units (Zones 1 and 2). In addition, the shallow aquifer (Zone 3), where the contamination plume will be first detected, will be subjected to a rigorous regime of investigation and monitoring campaigns for local remediation-related objectives, which will provide detailed information about its hydraulic and transport properties that can be effectively utilized in source identification analysis. However, for Zones 1 and 2, only some soft data (e.g., geophysical surveys) describing the heterogeneity architecture of their permeability field was assumed to be known.

Different techniques and scales of parameterization were adapted to represent model parameters under each tested uncertainty scenario towards a holistic and more representative inclusion of model input uncertainty with the Bayesian inverse problem. Table 2 presents the initial values, lower/upper bounds, and the used parameterization technique with the considered adjustable parameters in each uncertainty scenario.

The uncertainty in the storage formation flow gradient and permeability field was represented in the inverse problem by allowing the constant head BC and K-field of Zone 1 to vary within the bounds presented in Table 2. The BC nodes of Zone 1 were represented in the inverse problem using a single constant parameter, while the K-field of Zone 1 was represented using 77 spatially distributed pilot points (Fig. 3). Such pilot points assign the K values to mesh elements using kriging interpolation based on a predefined exponential covariance. The covariance parameters (i.e., range = 11.2 cm and sill =1.1) and

Table 2 Priori parameter summary.

Parameter Type	Count	Initial Value ⁴	Lower Bounds	Upper Bounds	Parameterization method	Uncertainty Scenarios ¹	Notes/Comments
Zone 1 BCE (m)	1	1.8	1.6	2	Constant parameter	1 and 7	Only the upper constant head of Zone 1 was adjustable.
Zone 1 K-field (m/d)	77	150	5	445	Pilot points parameters	2 and 7	Staggery distributed PPs with maximum spacing of 7 cm was implemented (Fig. 3)
Fractures' Ks (m/d)	6	250	1	500	Constant parameters	3 and 7	Wide range of the fracture permeabilities was given.
Fractures' widths (m)	12	Varies ²	Varies ²	Varies ²	Mobile/Dynamic parameters	3 and 7	The y-coordinates of the six fractures' edges were adjustable within the limits shown in Fig. 3.
Zone 2 K-field (m/d) (Lay: 1, 5, 9, 13) ³	4	296	148	445	Constant parameters	4 and 7	The permeability of the 16 overlaying units were parameterized as constant zones (Fig. 3).
Zone 2 K-field (m/d) (Lay.: 2, 6, 10, 14) ³	4	152	85	219	Constant parameters	4 and 7	
Zone 2 K-field (m/d) (Lay: 3, 7, 11, 15) ³	4	86	40	132	Constant parameters	4 and 7	
Zone 2 K-field (m/d) (Lay: 2, 8, 12, 16) ³	4	26	10	42	Constant parameters	4 and 7	
Zone 2 Porosity-field (-)	16	0.3	0.01	0.6	Constant parameters	5 and 7	The porosity of the 16 overlaying layers were parameterized as constant zones (Fig. 3)
Long. and Trans Dispersivity (m)	2	5.05E-04	1.00E-05	1.00E-03	Constant parameters	6 and 7	Constant longitudinal and transversal dispersivities for the whole system were assumed
Source location (m)	1	1	0.65	1.53	Mobile/Dynamic parameters	1 to 8	Only the y-coordinate of the source location was set adjustable, while the x-coordinate was calculated using the equation of $x=y+1.052$.
Leakage/Injection Rate (mL/min)	1	7.5	6	10	Constant parameter	1 to 8	Leakage rate was applied to the selected mesh elements by the source location parameter

Scenarios are described in Section 2.4

⁴ For all parameters except Zone 1 K-field, the initial values were derived by calculating the mean between the upper and lower limits.

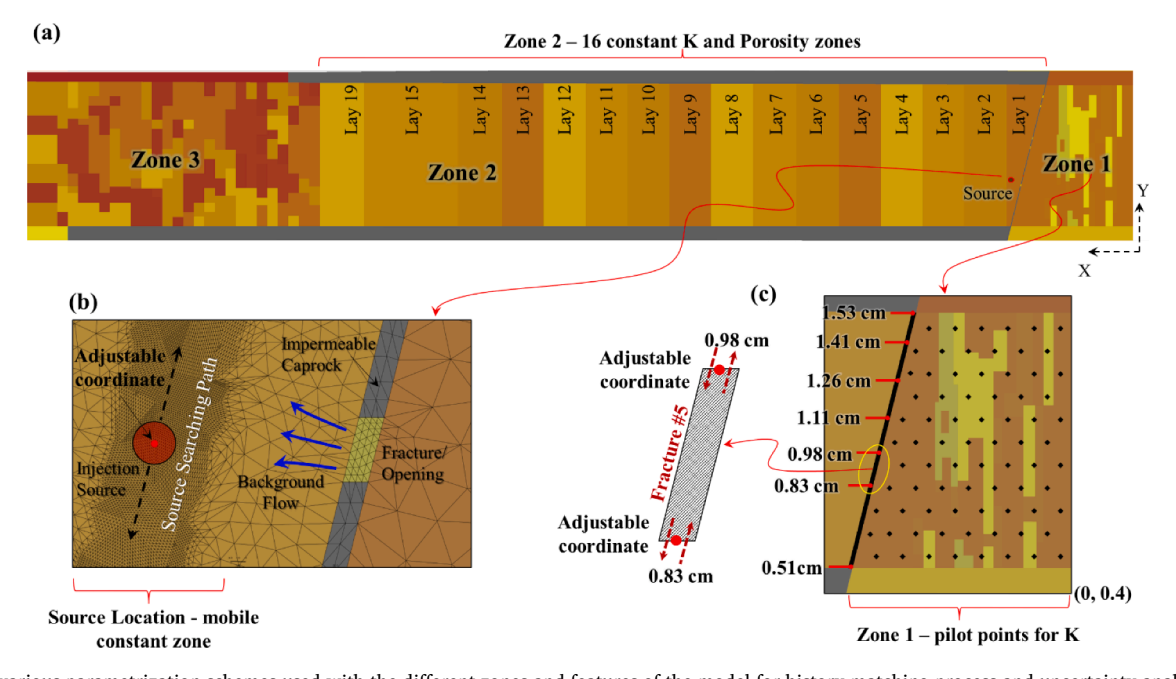


Fig. 3. The various parametrization schemes used with the different zones and features of the model for history matching process and uncertainty analysis. (a) The 16 constant-zone parameters used for representing Zone 2 layers. (b) The Mobile/Dynamic constant zone used for source searching. (c) The expandable constant zones used for parameterizing the caprock openings/fractures.

anisotropy structure of the actual heterogeneity in Zone 1 were assumed to be known, as in the field, feasible geophysical techniques can be used to estimate these statistical parameters (Yu et al., 2008; Nalonnil and Marion, 2012). The bounds of the K-field pilot points were determined based on the maximum and minimum K values resulted from column-scale tests for the packed types of sand in Zone 1. The initial values of the K-field pilot points were set equal to the column-scale estimated K for the most dominant sand type in Zone 1.

The hydraulic properties of Zone 2 (i.e., K and porosity) were parametrized using piecewise-constant parameter zones (Fig. 3a), as in the field, different seismic geophysical survey methods could be employed to map the overlying formations' interfaces with acceptable accuracy (Zweigel et al., 2004; Torp and Gale, 2004; Hermanrud et al., 2009). Column-scale estimated K and porosity values for the sand types used in Zone 2 were utilized to determine the bounding values for these constant parameters. It should be noted that the porosity of Zone 1 was

² Fracture edges' bounds are presented in Fig. 3c

³ Lay stands for layer, and Zone 2 layers are presented in Fig. 3a.

not parameterized as it was outside the transport domain of the NaBr migration.

The fractured caprock (i.e., openings width and K) and source settings (i.e., injection/leakage location and rate) were parametrized in the inverse problem using a novel approach referred to herein as the "Mobile/Dynamic Constant Zones" (MDCZs). Such MDCZs were used to introduce flexibility in the constant zone size and position across the model domain or within specific areas. For example, the fracture widths were parameterized using six expandable and mobile rectangular zones that assign constant high K values (i.e., K-fractures) to the caprock meshelements located within each of these zones. The coordinates of the upper and lower edges of these rectangular zones were set as parameters to be varied by PESTPP-IES within the limits presented in Fig. 3c and Table 2. By that, the caprock fracture sizes and locations can be counted as adjustable parameters in the inverse problem during history-matching.

The same technique was adapted to parametrize the source settings (i.e., leakage location and rate), where a circular zone with a radius of 0.3 cm was allowed to roam the area downstream the injection point and then select a set of mesh elements to assign constant mass flux BC to represent tracer injection (i.e., leakage source) (Fig. 3b). The coordinates of the circular zone center (i.e., x and y) were determined by a linear function (i.e., x=-y+1.052), where the y-coordinate was the only adjustable parameter by PESTPP-IES. Notably, the source size (the circular zone radius) was assumed known since the size of the potentially leaking fractures in the caprock can be predicted using geomechanical modeling (Feng et al., 2018). Collectively, the parameterization of both caprock fractures and source settings work together to represent a wide range of source-leakage configurations.

As discussed in Section 2.4, complete knowledge about the shallow aquifer hydraulic properties and sand heterogeneity was assumed. Thus, Zone 3 was not parameterized for the present UA and the calibrated parameters of Askar et al. 2021a were fixed for this zone in the UA. Finally, two constant zones were used to represent the longitudinal and transversal dispersivities for the whole system. By that, a total of 132 parameters were included in the UA performed in this study.

2.6. Data assimilation and observations

The ultimate goal of the conducted analysis herein is to reduce the uncertainty in our prior knowledge about leakage/injection source and rate (denoted as leakage source and rate henceforth) through data assimilation process (Doherty and Moore, 2019). To achieve this goal, a total of 1315 concentration data points and 30 head records from the tank experiment were used as observations for history matching. A subjective likelihood function was applied through assigning observation weights that first guarantee balanced contributions from all data types towards the objective function and second emphasize the importance of fitting the zero concentration points located outside the plume body. These zero concentration data points were given weights three times larger than of those assigned to the rest of the concentration data. By that, we focus the data assimilation process on preferentially reproducing the plume migration pathway over precisely predicting the inner concentration distribution of the plume in attempt to reduce the uncertainty in the leakage source location and rate predictions (Doherty and Welter, 2010).

2.7. Implementation and evaluation

The source identification approach outlined in Section 2.3 was implemented under an ensemble size of 500 realizations, which was considered reasonable given the available computational capacity at the time of conducting this study. The prior parameter ensemble was locally evaluated using PESTPP-IES through running a python script, based on FEFLOW-IFM that takes each realization parameters and map them to the base-model, run the simulation, and post-process the results.

Minimum of four PESTPP-IES iterations, including the base run (i.e., zero-iteration) were performed for data-assimilation process and history-matching prior parameters to observed data.

Since the problem under study does not include time-dependent parameters (e.g., extraction rates and recharge), the automatic adaptive localization, encoded in PESTPP-IES (White et al., 2020; Luo and Bhakta, 2020), was considered adequate to remove any statistically spurious correlations between parameters and observations.

It should also be noted that PESTPP-IES was set up to iteratively omit any non-behavioral realizations from the data-assimilation analysis; non-behavioral realizations can be defined as the ones that result in a phi value (objective function output) that exceeds the ensemble mean-phi plus two standard divisions (STDs). Moreover, the observations that showed statistically significant conflict with model outputs (i.e., their residuals were larger than three STDs from the mean of all simulated values across the prior simulated ensemble for a given observation), were removed from the data-assimilation process as well. Finally, the parameter realizations that took larger than twofold of the average run time of the entire ensemble were stopped and treated as failed runs in history-matching. Readers are referred to White et al. (2020) for more information about the available options in PESTPP-IES to setup a well constrained high-dimensional inverse problem.

The history-matching results were evaluated by calculating the Average Normalized Root Mean Square (ANRMS) at every observation point and then plot the results over the tank domain for comparison. The ANRMS was estimated by determining the root mean square error (RMSE) of the simulated data at each observation point and then normalize it on the maximum observed value of this type of observation (e.g., concentration and head data) and finally take the average of the normalized RMSEs over the ensemble size. The RMSE was normalized so that the concentration and head data are comparable in the same plot in terms of data-fitting goodness. Equation 1 presents the components of the calculated ANRMS for each observation point used in this analysis.

$$ANRMS = \sum_{1}^{n_{T}} \frac{\sqrt{\sum_{1}^{n_{R}} (S_{m} - S_{o})^{2}}}{S_{max}} / n_{T}$$
 (1)

where S_m , S_o and S_{max} are respectively the simulated, observed, and maximum values of the system state variable of interest (e.g., head and concentration). While n_R and n_T are the number of realizations and observed data points over time at each monitoring port.

3. Results and discussion

In this section, the results of history-matching and source identification under both cases of data availability (i.e., shallow, and relatively-deep datasets) are presented and discussed.

3.1. History matching

Data-assimilation leverage and data-fit are presented graphically by plotting both the phi trajectories for every ensemble member after 4 iterations of data assimilation (besides the base run) and the ANRMS for all observation points under each uncertainty scenario (Figs. 4 and 5). It should be noted that these plots were developed and discussed for the shallow-data case only, as this case contains the least amount of information and yields the largest posterior uncertainties, thus representing the worst conditions for data-availability.

Fig. 4 shows that shallow observed data can condition model parameters and reduce the prior ensemble phi several orders of magnitude under all uncertainty scenarios except scenarios 2 and 8. The results of scenario 8 suggest that treating source settings as the only source of model-input uncertainty (i.e., leakage location and rate) does not provide enough degrees of freedom to fit shallow observed concentration

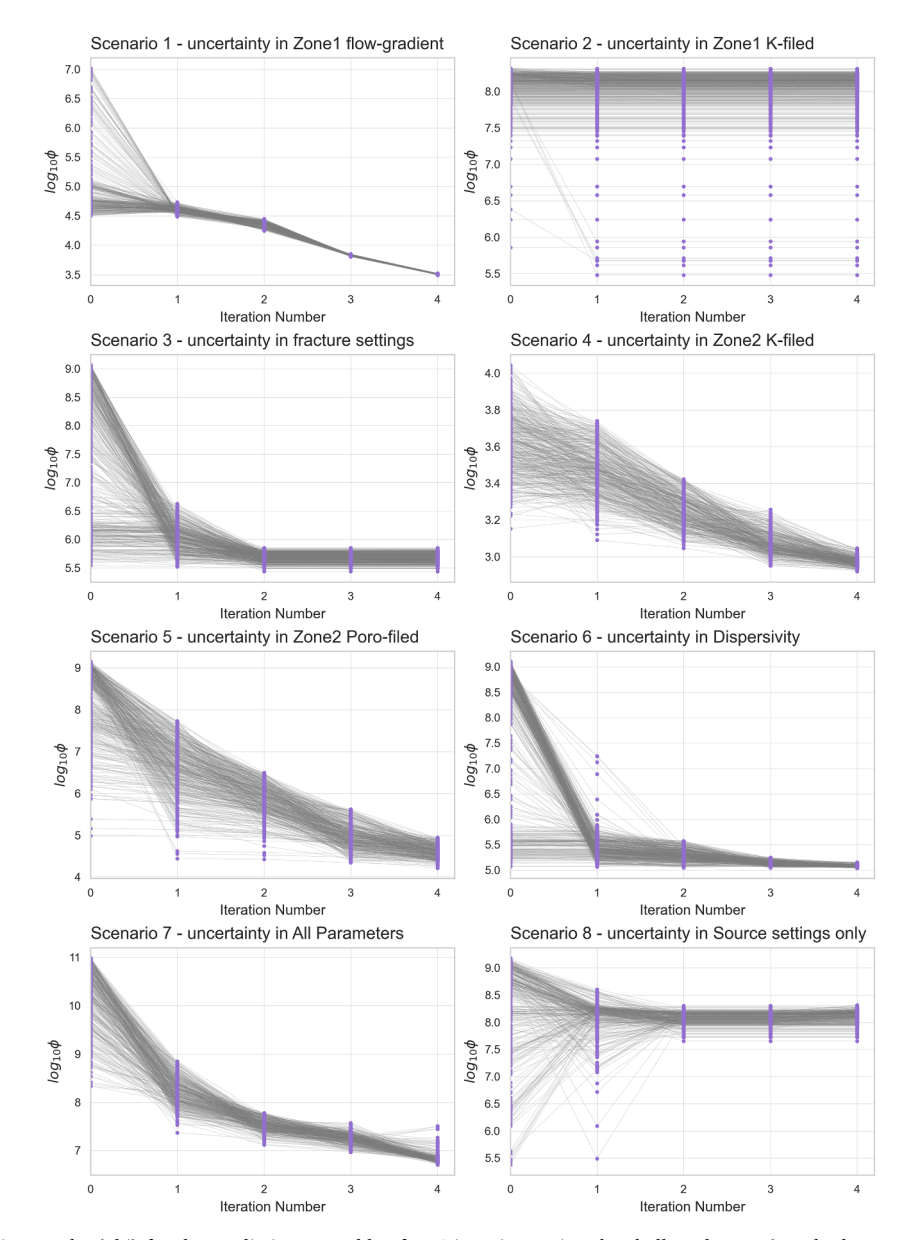


Fig. 4. The objective function results (phi) for the predictive ensemble after 4 iterations using the shallow dataset (purple dots represent the start and end of a single iteration).

data, evidence of the importance of considering source, property, and BC uncertainty simultaneously. As varying the source settings may alter the overall migration pathway and plume shape, as discussed by Askar et al. (2021a), but cannot change the inner concentration distribution of the plume in the shallow aquifer.

By incorporating the K-field of Zone 1 to the parameterization scheme with source settings (Scenario 2), a markedly less reduction in the phi was obtained. This can be attributed to two main factors. First, the counter-interaction between the effects of changing Zone 1 K-field and source settings, which basically comes from the great effect that Zone 1 K-field can have on the local flow field at the source vicinity (Askar et al., 2021a). For example, placing a low-permeability area in Zone 1 below the fractures/openings repeals the effect of increasing the leakage rate. Second, the significant nonlinearity imposed by Zone 1 K-field in the parameters-data relationship; the sensitive portion of K-field towards data continuously varies with source location adjustment, which affects the data-assimilation efficiency. For instance, when PESTPP-IES moves the source location to the top part of the tank, the most sensitive portion of the K-field becomes the upper section of Zone 1

and vice versa. In contrast, adding Zone 1 BCE to the parameterization scheme (Scenario 1) enhances the phi reduction (Fig. 4), as it does not introduce the same nonlinearity as the Zone-1 K-field.

The maximum reduction in phi was found under scenarios 3, 5, and 6, which included the fracture/opening settings, Zone 2 porosity, and entire model dispersivity, respectively. The reasonable data-fitting resulted under these scenarios was due to the significant effect of the considered parameters on plume propagation velocity (porosity and fracture settings) and concentration distribution (dispersivity and fracture settings), which both are essential to fully assimilate the information in the shallow-aquifer (Zone 3). However, when all parameters were included in the calibration process, a less reduction in phi was obtained because of the complexity added to the solution space by the high nonlinearity introduced to the inverse problem in this scenario and the counter-interaction between the effects of some parameters, as discussed earlier.

The effect of limited phi reduction in scenarios 2 and 8 can also be seen in Fig. 5, where the ANRMS of concentration data (marked by circles) was considerably high for most monitoring locations in these

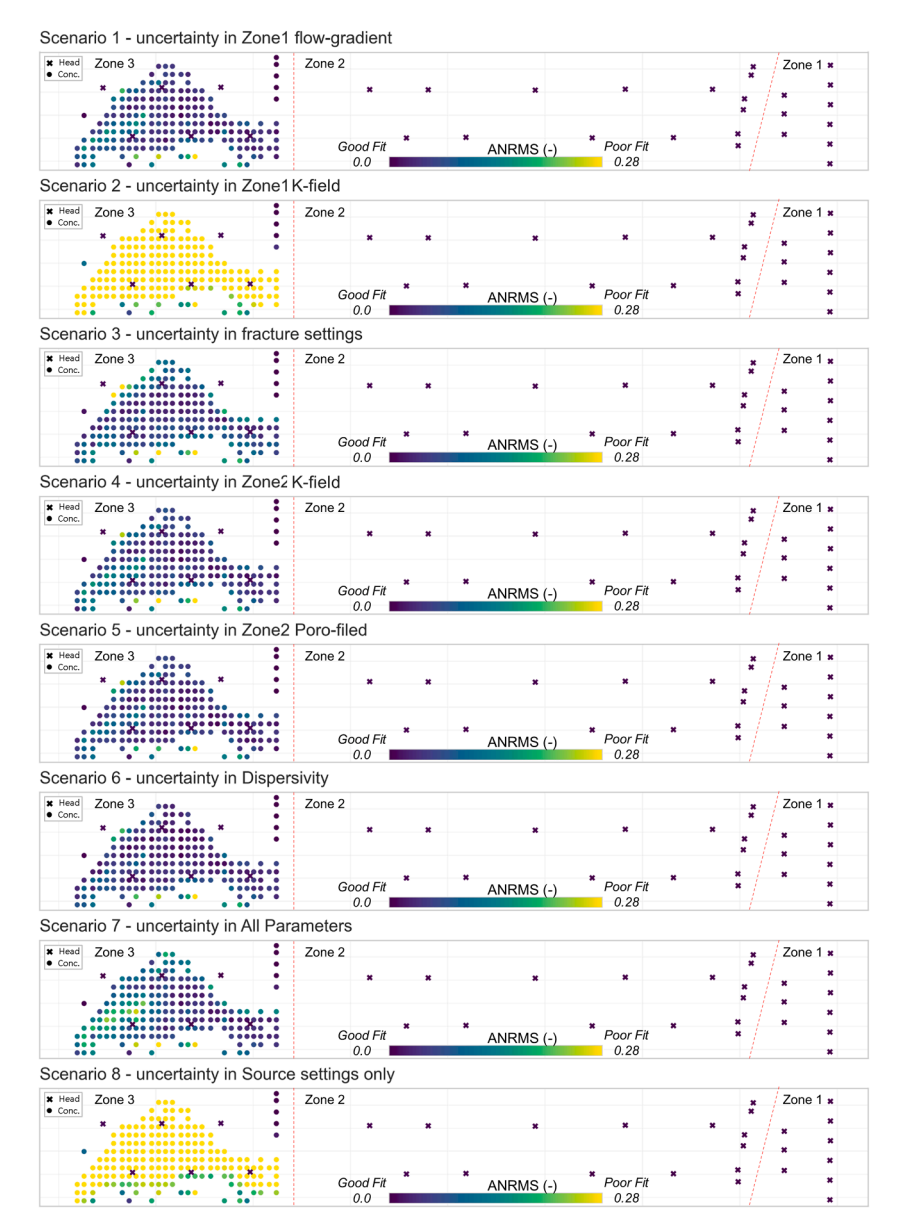


Fig. 5. The average normalized root mean square (ANRMS) of observed data residuals at each monitoring port in the tank after 4 iterations using the shallow dataset.

scenarios compared to others. However, head data (marked by crosses) was reasonably fitted under all scenarios. This suggests the high sensitivity of head data to the source settings and Zone 1 K-field compared to concentration data due to the proximity of deep head data to the source vicinity and deep formation (Zone 1), which is in good agreement with the findings of Askar et al. (2021a; 2021b). Fig. 5 also shows that the zero concentration points located at the shallow aquifer entry (Zone 3 deep section) were reasonably fitted in all scenarios due to the large weight given to them, which helps in reproducing the plume migration pathway and thus finding an improved simulated location of the leakage.

3.2. Source characterization

The accuracy of source identification and leakage rate prediction was evaluated by comparing the posterior distributions of these parameters with their true values (e.g. source y-coordinate and injection rate). Figs. 6 and 7, respectively show the prior (gray bars) and posterior (purple bars) histograms of the predictions of interest in this analysis (i. e., source location and leakage rate) relative to the true values measured

during the experiment. In general terms, all scenarios revealed a reasonable reduction in the source location uncertainty and almost zero change in the prior uncertainty of the leakage rate, with some scenarios showing biased estimates of the leakage rate.

Results demonstrate that shallow data was able to reduce the uncertainty associated with the prior knowledge of source location by more than $\sim\!70\%$ under all scenarios while maintaining a reasonable bracketing of the true y-coordinate (i.e., 0.803 m). Moreover, less than 10% error was obtained in the mean of estimated source locations across the posterior ensemble, indicating a high sensitivity of this parameter to the shallow data used in this analysis. The largest uncertainty reduction and smallest error in the posterior ensemble mean of leakage location were found under scenarios number 6, 5, 4, and 3 reflecting the impact of history matching on source identification. This suggests the importance of including system dispersivity, fracture settings, overlaying formations' porosities and permeabilities in the inverse problem for better source characterization outcomes.

On a different note, source characterization results show that with the relatively poor fitting of the data under scenarios 2 and 8 (as discussed above), PESTPP-IES could still reasonably narrow the possible

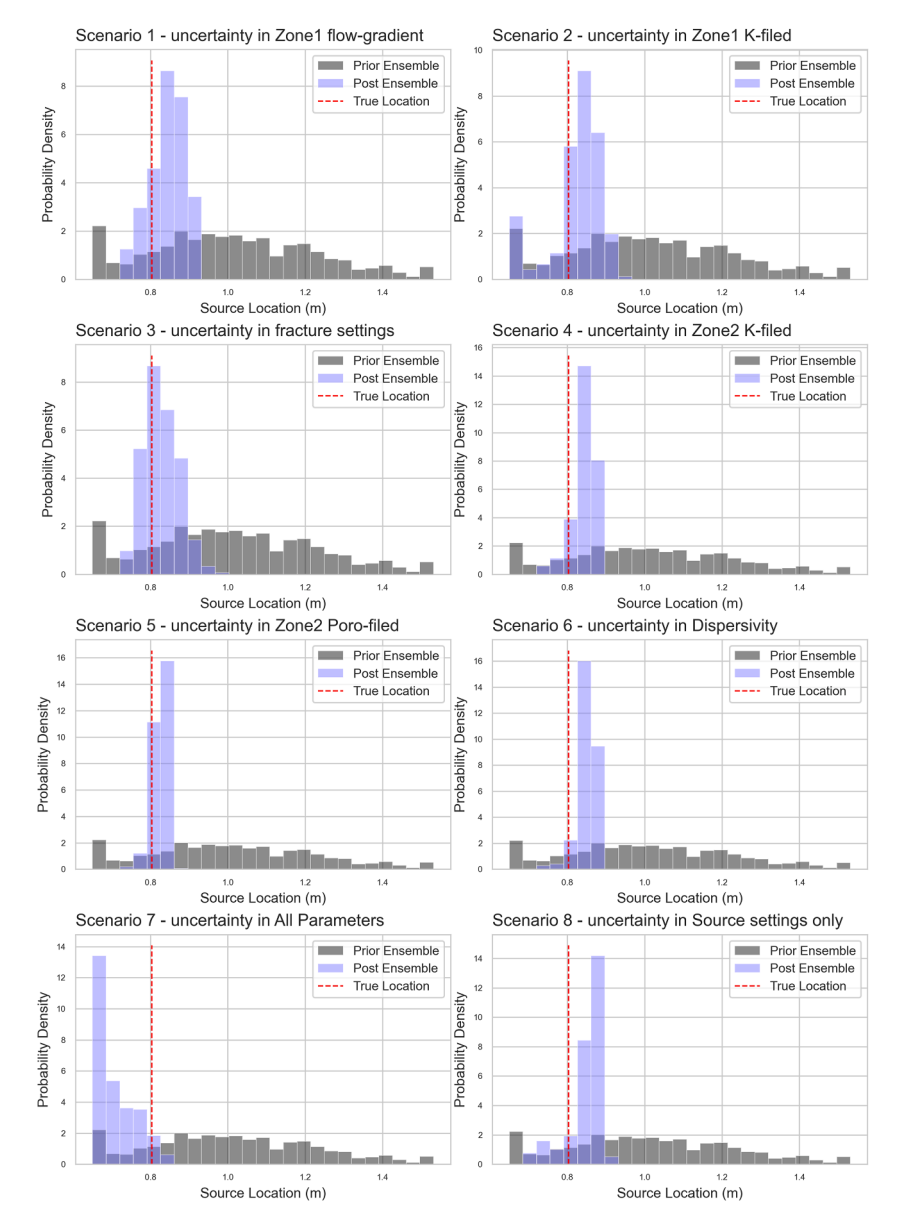


Fig. 6. The prior and posterior (post) parameter ensemble of source location, after 4 iterations using shallow dataset, with the true value represented by the red dashed line. All scenarios include uncertainty in source settings.

range of leakage source locations. Therefore, a high degree of data fitting may not be needed for source identification, which can significantly reduce the computational burden of the history-matching process. It should also be noted that under extreme uncertainty conditions in model parameters (scenario 7), PESTPP-IES was still capable of identifying a fair accurate range of possible source location.

As evidenced by the parameterization scenarios tested, the degree of biasness in the leakage rate estimates can be attributed to inappropriately reducing or removing otherwise uncertain model inputs from the data assimilation process. When uncertain parameters are removed from the data assimilation process, the information contained in the observation data that would have conditioned these missing parameters is now erroneously used to condition the remaining adjustable parameters. This erroneous adjustment is referred to in the literature as "parameter compensation" (Clark and Vrugt, 2006; White et al., 2014). Note that this parameter compensation cannot be detected in more traditional inverse problem settings, where the true value of the parameters is not known.

Regarding leakage rate characterization, either a very limited uncertainty reduction or an erroneous estimate was obtained. In scenarios 3, 5 and 6, where a reduction of more than 70% was obtained in the prior uncertainty, an error of more than 20% in the mean of estimated leakage rates across the posterior ensemble was resulted. While for all other scenarios, a significantly small uncertainty reduction, less than 20%, was achieved, reflecting a limited informativity of the shallow data to the deep leakage rate parameter. Hence, we decided to extend this analysis and investigate the impact of data proximity to the source on the identification accuracy of the leakage location and rate. Fig. 8 presents the source characterization results for scenarios 7 and 8 after adding the relatively-deep dataset (Fig. 1) to the calibration targets used in the previous UA and history matching (i.e., shallow data). Such analysis represents the testing of the 2nd data-availability case described in Section 2.4.

Fig. 8 shows a slight enhancement in source location identification under scenario 7 (78% instead of 74% uncertain reduction) by incorporating the relatively-deep data in history matching. However, an extra 20% of reduction in the source location uncertainty was obtained under scenario 8 compared to the previous shallow-data-only based analysis. With these improvements, the source location estimates across the posterior ensemble in both scenarios 7 and 8 were still reasonably

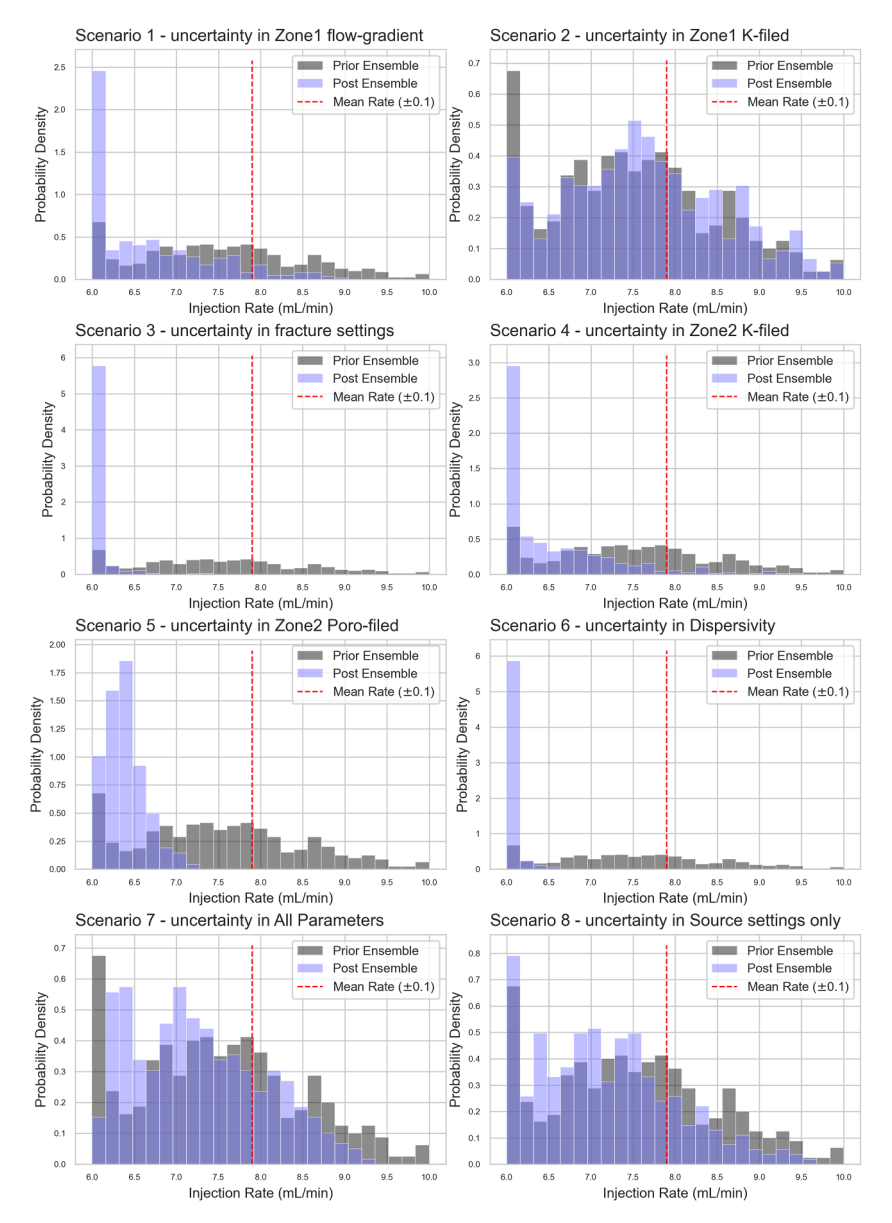


Fig. 7. The prior and posterior (post) parameter ensemble of leakage rate, after 4 iterations using shallow dataset, with the true value represented by the red dashed line. All scenarios include uncertainty in source settings.

bracketing the true value with an error less than 7% in the ensemble mean. For the leakage rate, the additional deep data did not provide better uncertainty reduction for scenario 7 but at least it was able to mitigate the parameter compensation and thus not providing an erroneous estimate of the leakage rate range. This indicates how hard it is to predict the leakage rate under field conditions where many aspects of the system are uncertain, which was confirmed by the results of scenario 8, where a significant decrease in the uncertainty of the leakage rate was obtained (84% instead of 15% uncertain reduction).

3.3. Summary discussion

The above analysis highlighted the possibility of characterizing the leakage source settings, in terms of location and rate, under uncertainty conditions using PESTPP-IES. Relatively inexpensive shallow data was found adequate to identify the most probable range of leakage source location, even under low degree of data-fitting. However, estimating the leakage rate was more challenging using shallow data only and the results revealed that deeper data with additional prior knowledge about the system properties are needed for accurate assessment of the leakage

rate. Hence, it is recommended to use the easily available shallow data to obtain a rough estimate of the possible locations of the leakage and then perform additional targeted data collection at these locations to acquire data that can help accurately estimating the leakage rate. By that, the cost of pre-remediation investigation work will be significantly reduced, which can be critical for operators and environmental authorities.

In field settings, multiple potential leakage sources may exist due to the extended size of the injection-pressure footprint (Birkholzer et al., 2009, 2011; Cavanagh and Wildgust, 2011). To account for such conditions, a large number of MDCZ parameters may be needed in modeling analysis to search for and identify all possible leakage sources in the caprock that may individually or collectively provide a good match to the data. Such augmentation in the parameter space can significantly increase the ill-posedness of the inverse problem, which can affect the ability to uniquely identify the "true" leakage settings' ranges. For that, geo-mechanical models can be incorporated in the UA process to reduce the solution space size through identifying the most critical zones in the caprock (Min et al., 2004; Rutqvist et al., 2007; 2008; Pan et al., 2013; Figueiredo et al., 2015; Feng et al., 2018). Several geophysical

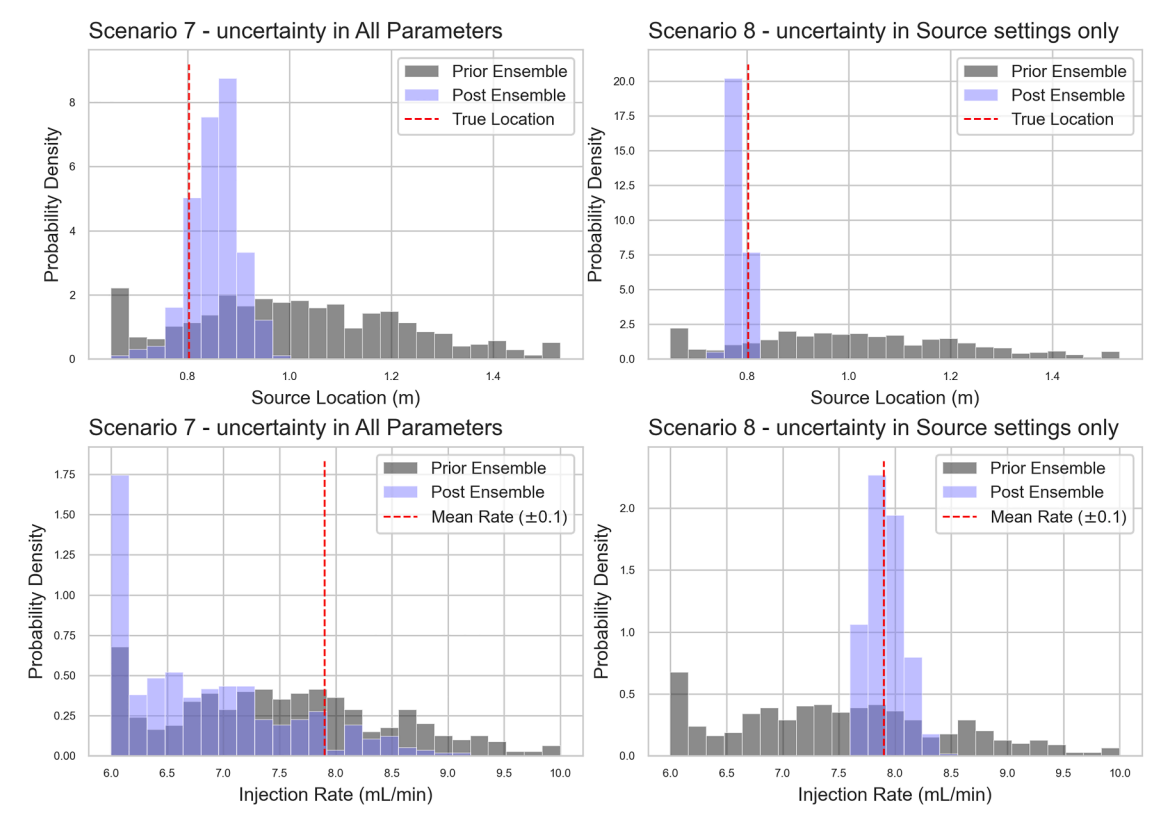


Fig. 8. The prior and posterior (post) parameter ensemble of source location and leakage rate, after 4 iterations using relatively-deep dataset, with the true values represented by the red dashed lines. All scenarios include uncertainty in source settings. Both shallow and relatively deep datasets were used in generating these results.

techniques can also be used to find the potential sites of pressure-driven fractures in the top seal of CO₂ storage confining layer (Ingram and Urai, 1999; Ligtenberg 2005; Lohr et al., 2008; Krawczyk et al., 2015; Ziesch et al., 2019).

Finally, it should be pointed out that the use of the validated approach in this study could be extended to identify the source location and discharge-history of a contaminant in the shallow aquifers for applications less complicated than CGS. In that case, an improved performance of PESTPP-IES can be expected due to the plenty of available data and better-known system properties.

4. Conclusions

This study explored and validated the capabilities of the inversion tool "PESTPP-IES" to characterize the source settings (i.e., location and rate) of brine leakage from CO₂ storage formations under considerable margin of uncertainty in the system properties and limited available data. We basically tested the technical feasibility of using less expensive shallow data to condition model parameters and thus identify the leakage source settings. The data used in this study was generated by Askar et al. (2021a) using an intermediate-scale experiment conducted in an ~8 m long soil-tank. A base-model that reproduces the leakage migration in the tank was developed using FEFLOW as a process-based simulator within a formal data assimilation through history-matching performed using an iterative ensemble smoother. Besides a set of classical methods used to parameterize the system hydraulic properties, a novel approach was developed and employed to search the leakage source location and incorporate uncertainty in the caprock fractur sizes. For that, a technique called dynamic/mobile constant-zones was applied to set up parameters that can change in size and move across the model domain to select mesh elements/nodes for either assigning mass-flux BC (to prescribe a leakage source) or to introduce high-permeability areas into the caprock layer (to represent a facture/opening). A set of conclusions were derived from the conducted source characterization analysis in this study which can be summarized as follows:

- 1 Shallow data was informative enough to condition the base-model and reduce the prior uncertainty in source location by about 70% under all scenarios, highlighting the sensitivity of source location to near-surface, relatively inexpensive data.
- 2 Characterizing the leakage rate needed deeper data with higher level of prior knowledge about the system properties so that more reliable probability ranges can be obtained.
- 3 Such findings introduce the opportunity of using iterative ensemble smoother with shallow data to obtain a rough estimate of possible source locations, where extra site exploration work can be conducted to acquire deeper data and make reasonable prediction of the leakage rate.
- 4 Source identification results emphasized the importance of including the system dispersivity, fracture geometrical settings (i.e., sizes), overlaying formations' porosities and permeabilities as parameters in the inverse problem for better reduction in the leakage location uncertainty.
- 5 The history-matching results demonstrated that low-to-moderate degree of data fitting could be sufficient to identify the leakage source using shallow data, which minimizes the required computational resources for such analysis,
- 6 Caution must be taken while selecting the parameterization scheme, as some parameters together can introduce complexity into the dataassimilation process (e.g., storage zone permeability field with source settings) due to their counter-interactions,
- 7 The dynamic/mobile constant zones parameterization can be utilized to reduce the extent of the model domain, by representing the leakage source as a constant flux BC instead of a high-K zone in the cap-rock, which will significantly reduce the domain extent and thus

- the computational burden of the ensemble-based data assimilation process,
- 8 For the possibility of multiple damage zones existing in the caprock, geo-mechanical models can be coupled with transport models to reduce the size of the solution space for better performance of the data assimilation.

The authors are aware that due to the absence of field data, the findings of this study are based on lab-scale experimental data, which may make them not directly applicable to field-scale problems. However, the study results still provide useful insights regarding the potential applicability of the proposed approach (based on using an iterative ensemble smoother) to identify the leakage source settings for actual CGS sites. Notably, the conducted analysis in this study was not feasible using data either from actual or pilot CGS sites because simply such data is not available; there are no detected brine leakage events in any commercial-scale CGS site till now and well-engineered pilot sites are basically designed not to leak to test CO₂ trapping efficacy (Keating et al., 2010). Moreover, relying solely on error-free synthetic data to validate the proposed approach can also lead to questionable findings due to the limitations of numerical models to capture micro/sub-grid processes affecting plume migrations. By that, the only option left to develop this study was to use intermediate-scale experiments, which allows us to generate field-like data under fully controlled conditions of the system.

CRediT authorship contribution statement

Ahmad H. Askar: Conceptualization, Methodology, Validation, Visualization, Formal analysis, Resources, Investigation, Writing – original draft, Writing – review & editing. Jeremy T. White: Methodology, Investigation, Writing – review & editing. Tissa H. Illangasekare: Conceptualization, Methodology, Writing – review & editing.

Declaration of Competing Interest

The authors declare that they have no known competing financial interests or personal relationships that could have appeared to influence the work reported in this paper.

Data availability

Data used in this study is publicly available and stored in the HydroShare digital repository https://doi.org/10.4211/hs.557dc959947842eb8aaf5d5427a21be3.

Acknowledgements

The authors acknowledge the support of INTERA Inc. for this study, represented in providing the needed computational resources and allowing employees to conduct research work during normal working hours. We are also grateful for the NSF funding (Award# 1702060) that supported the experimental work which helped generating the data used in this research. Authors would like to express appreciation to DHI, USA for supporting this research by offering an academic license of FEFLOW.

References

- Agartan, E., 2015. Fundamental Study On the Effects of Heterogeneity On Trapping of Dissolved CO2 in Deep Geological Formations Through Intermediate-Scale Testing and Numerical Modeling. Colorado School of mines, Golden. PhD Dissertation.
- Ajayi, T., Gomes, J.S., Bera, A., 2019. A review of CO2 storage in geological formations emphasizing modeling, monitoring and capacity estimation approaches. Pet. Sci. 16 (5), 1–36.

- Aral, M.M., Guan, J., Maslia, M.L., 2001. Identification of contaminant source location and release history in aquifers. J. Hydrol. Eng. 6 (3), 225–234.
- Askar, A.H., Illangasekare, T.H., Ilie, A.M.C., 2021b. Monitoring brine leakage from deep geologic formations storing carbon dioxide: design framework validation using intermediate-scale experiment. Water Resour. Res. 57 e2021WR031005.
- Askar, A.H., et al., 2021a. Exploring the impacts of source condition uncertainties on far-field brine leakage plume predictions in geologic storage of CO2: integrating intermediate-scale laboratory testing with numerical modeling. Water Resour. Res. 57 e2021WR029679.
- Atmadja, J., Bagtzoglou, A.C., 2001. State of the art report on mathematical methods for groundwater pollution source identification. Environ. Forensics 2 (3), 205–214.
- Bachu, S., 2003. Screening and ranking of sedimentary basins for sequestration of CO2 in geological media in response to climate change. Environ. Geol. 44 (3), 277–289.
- Birkholzer, J.T., et al., 2011. Brine flow up a well caused by pressure perturbation from geologic carbon sequestration: static and dynamic evaluations. Int. J. Greenhouse Gas Control 5 (4), 850–861.
- Birkholzer, J.T., Zhou, Q., Tsang, C.F., 2009. Large-scale impact of CO2 storage in deep saline aquifers: a sensitivity study on pressure response in stratified systems. Int. J. Greenhouse Gas Control 3 (2), 181–194.
- Bixler, N.E., 1989. An improved time integrator for finite element analysis. Commun. Appl. Numer. Methods 5 (2), 69–78.
- Bjarkason, E. et al., 2020. Uncertainty Quantification of Highly-Parameterized Geothermal Reservoir Models Using Ensemble-Based Methods. s.l., World Geothermal Congress (p. 1).
- Cameron, D.A., Durlofsky, L.J., Benson, S.M., 2016. Use of above-zone pressure data to locate and quantify leaks during carbon storage operations. Int. J. Greenhouse Gas Control 52, 32–43.
- Cavanagh, A., Wildgust, N., 2011. Pressurization and brine displacement issues for deep saline formation CO2 storage. Energy Procedia 4, 4814–4821.
- Celia, M.A., Bachu, S., Nordbotten, J.M., Bandilla, K., 2015. Status of CO2 storage in deep saline aquifers with emphasis on modeling approaches and practical simulations. Water Resour. Res. 51 (9), 6846–6892.
- Celia, M.A., et al., 2011. Field-scale application of a semi-analytical model for estimation of CO2 and brine leakage along old wells. Int. J. Greenhouse Gas Control 5 (2), 257–269.
- Chen, Z., et al., 2022. Reconstructing the release history of a contaminant source with different precision via the ensemble smoother with multiple data assimilation. J. Contam. Hydrol. 21, 104115.
- Clark, M.P., Vrugt, J.A., 2006. Unraveling uncertainties in hydrologic model calibration: addressing the problem of compensatory parameters. Geophys. Res. Lett. 33 (6).
- Diersch, G.H.J., 2014. FEFLOW: Finite Element Modeling of flow, Mass and Heat Transport in Porous and Fractured Media. Springer Science & Business Media, Heidelberg doi, 10, 978-3.
- Dimov, I., Jaekel, U., Vereecken, H., 1996. A numerical approach for determination of sources in transport equations. Comput. Math. Appl. 32 (5), 31–42.
- Doherty, J., Moore, C., 2019. Decision support modeling: data assimilation, uncertainty quantification, and strategic abstraction. Groundwater 58 (3), 327–337.
- Doherty, J., Welter, D., 2010. A short exploration of structural noise. Water Resour. Res. 46 (5), W05525.
- Feng, J., et al., 2018. An improved geomechanical model for the prediction of fracture generation and distribution in brittle reservoirs. PLoS One 13 (11), e0205958 (1:28).
- Fienen, M.N., et al., 2022. Risk-Based Wellhead Protection Decision Support: a Repeatable Workflow Approach. Groundwater 60 (1), 71–86.
- Figueiredo, B., Tsang, C.F., Rutqvist, J., Niemi, A., 2015. A study of changes in deep fractured rock permeability due to coupled hydro-mechanical effects. Int. J. Rock Mech. Min. Sci. 79, 70–85.
- Friedlingstein, P., et al., 2019. Global carbon budget 2019. Earth System Science Data 11 (4), 1783–1838.
- Gasda, S.E., Bachu, S., Celia, M.A., 2004. Spatial characterization of the location of potentially leaky wells penetrating a geological formation in a mature sedimentary basin. Environ. Geol. 46 (6–7), 707–720.
- González-Nicolás, A., Baù, D., Alzraiee, A., 2015. Detection of potential leakage pathways from geological carbon storage by fluid pressure data assimilation. Adv. Water Resour. 86, 366–384.
- Gorelick, S.M., Evans, B., Remson, I., 1983. Identifying sources of groundwater pollution: an optimization approach. Water Resour. Res. 19 (3), 779–790.
- Gresho, P.M., Lee, R.L., Sani, R.L., Stullich, T.W., 1979. Time-dependent FEM Solution of the Incompressible Navier-Stokes equations in Two-And Three-Dimensions. lawrence livermore national laboratory, California University preprint UCRL-81323.
- Grobe, M., Pashin, J.C., Dodge, L.R., 2009. Carbon Dioxide Sequestration in Geological Media—State of the Science, 1st ed. American Association of Petroleum Geologists, Tulsa, OK.
- Hermanrud, C., et al., 2009. Storage of CO2 in saline aquifers-lessons learned from 10 years of injection into the Utsira Formation in the Sleipner area. Energy Procedia 1 (1), 1997–2004.
- Hovorka, S.D., Meckel, T.A., Treviño, R.H., 2013. Monitoring a large-volume injection at Cranfield, Mississippi—Project design and recommendations. Int. J. Greenhouse Gas Control 18, 345–360.
- Ingram, G.M., Urai, J.L., 1999. Top-seal leakage through faults and fractures: the role of mudrock properties. Geol. Soc. 158 (1), 125–135. , London, Special Publications.
- IPCC, 2005. IPCC Special Report on Carbon Dioxide Capture and Storage. Prepared by Working Group III of the Intergovernmental Panel on Climate Change [Metz, B., O. Davidson, H. C. de Coninck, M. Loos, and L. A. Meyer (eds.)], Cambridge, United Kingdom and New York, NY, USA, 442 pp. s.n.

- Jiang, S., et al., 2022. Simultaneous Estimation of a Contaminant Source and Hydraulic Conductivity Field by Combining an Iterative Ensemble Smoother and Sequential Gaussian Simulation. Water 14 (5), 757.
- Jung, Y., Zhou, Q., Birkholzer, J., 2013. Early detection of brine and CO2 leakage through abandoned wells using pressure and surface-deformation monitoring data: concept and demonstration. Adv. Water Resour. 62, 555–569.
- Keating, E., et al., 2010. The impact of CO2 on shallow groundwater chemistry: observations at a natural analog site and implications for carbon sequestration. Environ. Earth Sci. 60 (3), 521.
- Knowling, M.J., White, J.T., Moore, C.R., 2019. Role of model parameterization in risk-based decision support: an empirical exploration. Adv. Water Resour. 128, 59–73.
- Krawczyk, C., et al., 2015. Seismic and sub-seismic deformation prediction in the context of geological carbon trapping and storage. Geological Storage of CO2–Long Term Security Aspects. Springer, Cham, pp. 97–113.
- Kugler, B., Forbes, F., Douté, S., 2022. Fast Bayesian Inversion for high dimensional inverse problems. Stat Comput 32 (2), 1–23.
- Lackner, K.S., 2003. A guide to CO2 sequestration. Science 300 (5626), 1677–1678.
 Ligtenberg, J.H., 2005. Detection of fluid migration pathways in seismic data:
 implications for fault seal analysis. Basin Res. 17 (1), 141–153.
- LIU, J.B., et al., 2021. Groundwater contaminant source identification based on QS-ILUES. J. Groundwater Sci. Eng. 9 (1), 73–82.
- Lohr, T., et al., 2008. Prediction of subseismic faults and fractures: integration of three-dimensional seismic data, three-dimensional retrodeformation, and well data on an example of deformation around an inverted fault. Am. Assoc. Pet. Geol. Bull. 92 (4), 473-485
- Looney, B., 2020. Statistical Review of World Energy. Edition: 69: Bp.
- Luo, X., Bhakta, T., 2020. Automatic and adaptive localization for ensemble-based history matching. J. Pet. Sci. Eng. 184, 106559.
- Luyun Jr, R., Momii, K., Nakagawa, K., 2011. Effects of recharge wells and flow barriers on seawater intrusion. Groundwater 49 (2), 239–249.
- Mahar, P.S., Datta, B., 2000. Identification of pollution sources in transient groundwater systems. Water Resour. Manage. 14 (3), 209–227.
- Mahar, P.S., Datta, B., 2001. Optimal identification of groundwater pollution sources and parameter estimation. J. Water Resour. Plann. Manage. 127 (1), 20–29.
- Mahinthakumar, G., Sayeed, M., 2005. Hybrid genetic algorithm—Local search methods for solving groundwater source identification inverse problems. J. Water Resour. Plann. Manage. 131 (1), 45–57.
- Ma, W., Jafarpour, B., Qin, J., 2019. Dynamic characterization of geologic CO2 storage aquifers from monitoring data with ensemble Kalman filter. Int. J. Greenhouse Gas Control 81, 199–215.
- Milnes, E., Perrochet, P., 2007. Simultaneous identification of a single pollution pointsource location and contamination time under known flow field conditions. Adv Water Resour 30 (12), 2439–2446.
- Min, K.B., Rutqvist, J., Tsang, C.F., Jing, L., 2004. Stress-dependent permeability of fractured rock masses: a numerical study. Int. J. Rock Mech. Min. Sci. 41 (7), 1191–1210.
- Mortezaei, K., Amirlatifi, A., Ghazanfari, E., Vahedifard, F., 2018. Potential CO2 leakage from geological storage sites: advances and challenges. Environmental Geotechnics 8 (1) 3–27
- Nalonnil, A., Marion, B., 2012. High-resolution reservoir monitoring using crosswell seismic. SPE Reservoir Eval. Eng. 15 (01), 25–30.
- NETL, 2017. BEST PRACTICES: Monitoring, Verification, and Accounting (MVA) For Geologic Storage Projects DOE/NETL-2017/1847. National Energy Technology Laboratory, Anchorage, AK.
- Neupauer, R.M., Lin, R., 2006. Identifying sources of a conservative groundwater contaminant using backward probabilities conditioned on measured concentrations. Water Resour. Res. 42 (3), W03424 (1-13).
- Neupauer, R.M., Wilson, J.L., 1999. Adjoint method for obtaining backward-in-time location and travel time probabilities of a conservative groundwater contaminant. Water Resour. Res. 35 (11), 3389–3398.
- Neupauer, R.M., Wilson, J.L., 2001. Adjoint-derived location and travel time probabilities for a multidimensional groundwater system. Water Resour. Res. 37 (6), 1657–1668.
- Neupauer, R.M., Wilson, J.L., 2002. Backward probabilistic model of groundwater contamination in non-uniform and transient flow. Adv Water Resour 25 (7), 733–746.
- Nordbotten, J.M., Celia, M.A., Bachu, S., 2004. Analytical solutions for leakage rates through abandoned wells. Water Resour. Res. 40 (4).
- Omagbon, J., et al., 2021. Case studies of predictive uncertainty quantification for geothermal models. Geothermics 97, 102263.
- Pan, P., Rutqvist, J., Feng, X., Yan, F., 2013. Modeling of caprock discontinuous fracturing during CO2 injection into a deep brine aquifer. Int. J. Greenhouse Gas Control 19, 559–575.
- Rassam, D., et al., 2022. Stochastic Assessment of Groundwater Contamination Risks From Onshore Gas Development Using Computationally Efficient Analytical and Numerical Transport Models. Front. Water 3, 799738.

- Rutqvist, J., Birkholzer, J., Cappa, F., Tsang, C.F., 2007. Estimating maximum sustainable injection pressure during geological sequestration of CO2 using coupled fluid flow and geomechanical fault-slip analysis. Energy Convers. Manage. 48 (6), 1798–1807.
- Rutqvist, J., Birkholzer, J.T., Tsang, C.F., 2008. Coupled reservoir–geomechanical analysis of the potential for tensile and shear failure associated with CO2 injection in multilayered reservoir–caprock systems. Int. J. Rock Mech. Min. Sci. 45 (2), 132–143.
- Singh, R.M., Datta, B., 2007. Artificial neural network modeling for identification of unknown pollution sources in groundwater with partially missing concentration observation data. Water Resour. Manage. 21 (3), 557–572.
- Singh, R.M., Datta, B., Jain, A., 2004. Identification of unknown groundwater pollution sources using artificial neural networks. J. Water Resour. Plann. Manage. 130 (6), 506–514.
- SIO, 2023. The Keeling Curve. [Online] Available at: https://keelingcurve.ucsd.edu/[Accessed 1 1 2023].
- Skaggs, T., Kabala, Z., 1995. Recovering the history of a groundwater contaminant plume: method of quasi-reversibility. Water Resour. Res. 31 (11), 2669–2673.
- Srivastava, D., Singh, R.M., 2014. Breakthrough curves characterization and identification of an unknown pollution source in groundwater system using an artificial neural network (ANN). Environ. Forensics 15 (2), 175–189.
- Sun, W., Durlofsky, L.J., 2019. Data-space approaches for uncertainty quantification of CO2 plume location in geological carbon storage. Adv Water Resour 123, 234–255.
- Tadjer, A., Bratvold, R.B., 2021. Managing uncertainty in geological CO2 storage using Bayesian evidential learning. Energies 14 (6), 1557.
- Todaro, V., D'Oria, M., Tanda, M.G., Gómez-Hernández, J.J., 2021. Ensemble smoother with multiple data assimilation to simultaneously estimate the source location and the release history of a contaminant spill in an aquifer. J Hydrol (Amst) 598, 126215.
- Torp, T.A., Gale, J., 2004. Demonstrating storage of CO2 in geological reservoirs: the Sleipner and SACS projects. Energy 29 (9–10), 1361–1369.
- Trevisan, L., et al., 2017. Imaging and quantification of spreading and trapping of carbon dioxide in saline aquifers using meter-scale laboratory experiments. Water Resour. Res. 53 (1), 485–502.
- Tsang, C.F., Birkholzer, J., Rutqvist, J., 2008. A comparative review of hydrologic issues involved in geologic storage of CO2 and injection disposal of liquid waste. Environ. Geol. 54 (8), 1723–1737.
- U.S. DOE, 2015. Carbon Sequestration Atlas of the United States and Canada, Fifth Edition. Department of Energy/NETL, USA, p. 24.
- U.S. EPA, 2013. Geologic Sequestration of Carbon Dioxide: underground Injection Control (UIC) Program Class VI Well Testing and Monitroing Guidnace, EPA 816-R-13-001, s.l.: EPA: Office of Water.
- Vermeul, V., et al., 2016. An overview of the monitoring program design for the FutureGen 2.0 CO2 storage site. Int. J. Greenhouse Gas Control 51, 193–206.
- Wagner, B.J., 1992. Simultaneous parameter estimation and contaminant source characterization for coupled groundwater flow and contaminant transport modelling. J. Hydrol. 135 (1–4), 275–303.
- White, J., Doherty, J.E., Hughes, J.D., 2014. Quantifying the predictive consequences of model error with linear subspace analysis. Water Resour. Res. 50 (2), 1152–1173.
- White, J., Fienen, M. & Doherty, J., 2016. pyEMU: a python framework for environmental model uncertainty analysis, version .01, https://dx.doi.org/10.5066 /F75D8Q01: U.S. Geological Survey software release.
- White, J.T., 2018. A model-independent iterative ensemble smoother for efficient history-matching and uncertainty quantification in very high dimensions. Environ. Model. Softw. 109, 191–201.
- White, J.T., Hunt, R.J., Fienen, M.N. & Doherty, J.E., 2020. Approaches to highly parameterized inversion: PEST++ Version 5, a software suite for parameter estimation, uncertainty analysis, management optimization and sensitivity analysis (No. 7-C26), s.l.: US Geological Survey.
- Wu, K., Chen, P. & Ghattas, O., 2020. A fast and scalable computational framework for large-scale and high-dimensional Bayesian optimal experimental design. rXiv preprint arXiv:2010.15196.
- Xu, T., et al., 2022. Non-point contaminant source identification in an aquifer using the ensemble smoother with multiple data assimilation. J. Hydrol. 606, 127405.
- Yu, G., et al., 2008. Crosswell seismic imaging for deep gas reservoir characterization. Geophysics 73 (6), B117–B126.
- Zheng, N. et al., 2022. Identification of contaminant source and hydraulic conductivity field based on an ILUES-SOM surrogate model.
- Zhou, Q., et al., 2016. Early Detection of Brine and CO2 Leakage Using Pressure and Surface-Deformation Monitoring Data: Methodology Development, Demonstration, and Application, United States. National Energy Technology Laboratory (NETL). https://doi.org/10.18141/1433142.
- Ziesch, J., Tanner, D., Krawczyk, C., 2019. Subseismic pathway prediction by three-dimensional structural restoration and strain analysis based on seismic interpretation. Am. Assoc. Pet. Geol. Bull. 103 (10), 2317–2342.
- Zweigel, P., Arts, R., Lothe, A.E., Lindeberg, E.B., 2004. Reservoir geology of the Utsira Formation at the first industrial-scale underground CO2 storage site (Sleipner area, North Sea). Geol. Soc. 233 (1), 165–180. London, Special Publications.